Role of high-order anharmonicity and off-diagonal terms in thermal conductivity: A case study of multiphase $CsPbBr_3$

Xiaoying Wang,[1] Zhibin Gao,[1,*] Guimei Zhu,[2,†] Jie Ren,[3] Lei Hu,[1] Jun Sun,[1] Xiangdong Ding,[1] Yi Xia,[4,‡] and Baowen Li[5,6]

[1]*State Key Laboratory for Mechanical Behavior of Materials, Xi'an Jiaotong University, Xi'an 710049, China*

[2]*School of Microelectronics, Southern University of Science and Technology, Shenzhen 518055, People's Republic of China*

[3]*Center for Phononics and Thermal Energy Science, China-EU Joint Center for Nanophononics, Key Laboratory of Special Artificial Microstructure Materials and Technology, School of Physics Sciences and Engineering, Tongji University, Shanghai 200092, China*

[4]*Department of Mechanical and Materials Engineering, Portland State University, Portland, Oregon 97201, USA*

[5]*Department of Materials Science and Engineering, Department of Physics, Southern University of Science and Technology, Shenzhen 518055, People's Republic of China*

[6]*Paul M. Rady Department of Mechanical Engineering and Department of Physics, University of Colorado, Boulder, Colorado 80305-0427, USA*

(Received 28 December 2022; revised 23 May 2023; accepted 30 May 2023; published 20 June 2023)

We investigate the influence of three- and four-phonon scattering, perturbative anharmonic phonon renormalization, and off-diagonal terms of coherent phonons on the thermal conductivity of $CsPbBr_3$ phase change perovskite, by using advanced implementations and first-principles simulations. Our study spans a wide temperature range covering the entire structural spectrum. Notably, we demonstrate that the interactions between acoustic and optical phonons result in contrasting trends of phonon frequency shifts for the high-lying optical phonons in orthorhombic and cubic $CsPbBr_3$ as temperature varies. Our findings highlight the significance of wavelike tunneling of coherent phonons in ultralow and glasslike thermal conductivity in halide perovskites.

DOI: 10.1103/PhysRevB.107.214308

I. INTRODUCTION

Phonons are crucial for understanding thermal transport in semiconductors and dielectrics. In the traditional approach of first-principles calculations, important quantities such as the mode-Grüneisen parameter, thermal expansion, phonon group velocity, three-phonon lifetime, and linewidth can be obtained by using anharmonic lattice dynamics under the quasiharmonic approximation through the linearized phonon Boltzmann transport equation [1–3].

However, the traditional approach, in which some important factors have been overlooked, is facing several challenges as follows.

(1) The higher-order interatomic interactions like the fourth order have been ignored for a long time like in BAs in which the four-phonon scattering is responsible for around 40% suppression of κ_L compared to that with only three-phonon interactions.

(2) Interatomic anharmonicity increases as temperature is raised. However, the perturbation approach is difficult to deal with in highly anharmonic systems, such as cubic ABX_3 perovskites with imaginary frequencies of harmonic phonons [4,5]. Therefore, we should illustrate the significance of anharmonic phonon renormalization, by utilizing the self-consistent phonon (SCPH) with temperature-dependent frequencies in several systems [6,7].

(3) The off-diagonal terms in the heat flux operator representing the heat transfer through the tunneling of wavelike coherent phonons could provide a potential method to bridge the gap between the traditional Peierls-Boltzmann transport equation and the experimental measurement in ultralow thermal conductivity materials and glasslike materials [8]. Items (1) and (2) are related but independent from (3).

$CsPbBr_3$ is a classical chalcogenide material and a promising candidate for thermoelectric application, garnering significant attention in recent years. However, current studies have mainly focused on the thermal transport properties of individual phase [8,9], often considering only three-phonon scattering and calculating the lattice thermal conductivity with zero temperature phonon dispersion [10,11].

The systematic investigation of all three phases of $CsPbBr_3$, considering both renormalization effects and four-phonon scattering, as well as the contribution of off-diagonal terms, remains largely unexplored. Previous studies have primarily focused on phase transitions, vibrational mechanisms, and dielectric properties [12,13]. To the best of our knowledge, no systematic studies have been conducted to date that encompass all three phases while considering renormalization, four-phonon scattering, and off-diagonal contributions.

In this study, we conduct a systematic investigation of the influence of quartic anharmonicity on the lattice dynamics and thermal transport properties of the three distinct phases of $CsPbBr_3$. We employ recent advancements in first-principles

*zhibin.gao@xjtu.edu.cn
†zhugm@sustech.edu.cn
‡yxia@pdx.edu

simulations, incorporating (i) efficient construction of high-order interatomic force constants (IFCs) from the CSLD method [14–16], (ii) rigorous calculations of temperature-dependent phonons through SCPH theory and higher-order multiphonon scattering rates [4,17], and (iii) evaluation of the lattice thermal conductivity κ_L by using a unified theory that considers both diagonal terms from the standard Peierls contribution and off-diagonal terms from the coherent Wigner distribution [8,18].

II. COMPUTATIONAL METHODS

For the Peierls-Boltzmann transport equation, the lattice thermal conductivity κ_p can be calculated as

$$\kappa_p = \frac{\hbar^2}{k_B T^2 V N_0} \sum_{\lambda} n_\lambda (n_\lambda + 1) \omega_\lambda^2 \boldsymbol{v}_\lambda \otimes \boldsymbol{v}_\lambda \boldsymbol{\tau}_\lambda, \tag{1}$$

where $\hbar$, k_B, T, V, and N_0 are the reduced Planck constant, Boltzmann constant, absolute temperature, primitive unit cell volume, and the total number of sampled phonon wave vectors in the first Brillouin zone, respectively. n_λ, ω_λ, v_λ, and τ_λ are the equilibrium component of the phonon population, frequency, group velocity, and lifetime for the λ mode (wave vector q and branch index s), respectively. Except for τ_λ, all the above parameters can be obtained from harmonic approximation (HA). Usually, τ_λ can be obtained from the perturbation theory by consideration of three-phonon scattering [19,20].

The temperature-dependent phonon dispersion could be considered by the anharmonic phonon renormalization (APRN) at finite temperatures [22–27]. Among various existing approaches, SCPH [4,6] approximation is one effective method that can rigorously account for the first-order correction of phonon frequencies from the quartic anharmonicity. It can better describe the soft phonon modes and strong anharmonicity. In brief, under the SCPH approximation, the temperature-dependent renormalized phonon frequency Ω_λ can be obtained from the following equation:

$$\Omega_\lambda^2 = \omega_\lambda^2 + 2\Omega_\lambda \sum_{\lambda_1} I_{\lambda\lambda_1}, \tag{2}$$

where ω_λ is the original phonon frequency from the harmonic approximation. The scalar $I_{\lambda\lambda_1}$ can be obtained as

$$I_{\lambda\lambda_1} = \frac{\hbar}{8N_0} \frac{V^{(4)}(\lambda, -\lambda, \lambda_1, -\lambda_1)}{\Omega_\lambda \Omega_{\lambda_1}} \left[1 + 2n_\lambda\left(\Omega_{\lambda_1}\right)\right], \tag{3}$$

in which $V^{(4)}$ is the fourth-order IFCs in the reciprocal representation. The phonon population n_λ satisfies Bose-Einstein distribution as a function of temperature. Both Eq. (2) and Eq. (3) have parameters $I_{\lambda\lambda_1}$ and Ω_λ in common and thus the SCPH equation can be solved iteratively. Note that $I_{\lambda\lambda_1}$ can be interpreted as the interaction between a pair of phonon modes, λ and λ_1, including the temperature effects [4,6].

Moreover, if one considers the off-diagonal terms of the heat-flux operator, which depicts the tunneling of coherent phonons, an additional contribution of lattice thermal conductivity, κ_c, needs to be considered [28–30]. Usually, κ_c is neglected in simple crystals because of well-separated phonon dispersions and slight broadening as a function of temperature. However, it could dominate in disordered and glasslike amorphous compounds where phonon and related group velocities cannot be clearly defined and heat transfer is mediated by diffusons and locons [31–33].

Recent studies show that κ_c is substantial for materials with ultralow thermal conductivity, such as Mn_4Si_7 with twisting phonons [34], $Ba_{7.81}Ge_{40.67}Au_{5.33}$ clathrate [35], and Tl_3VSe_4 [36]. Therefore, in all-inorganic halide perovskite $CsPbBr_3$, we incorporate κ_c as follows:

$$\kappa_c = \frac{\hbar^2}{k_B T^2 V N_0} \sum_{\boldsymbol{q}} \sum_{s \neq s'} \frac{\omega_{\boldsymbol{q}}^s + \omega_{\boldsymbol{q}}^{s'}}{2} \boldsymbol{v}_{\boldsymbol{q}}^{s,s'} \otimes \boldsymbol{v}_{\boldsymbol{q}}^{s',s} \times \frac{\omega_{\boldsymbol{q}}^s n_{\boldsymbol{q}}^s \left(n_{\boldsymbol{q}}^s + 1\right) + \omega_{\boldsymbol{q}}^{s'} n_{\boldsymbol{q}}^{s'} \left(n_{\boldsymbol{q}}^{s'} + 1\right)}{4\left(\omega_{\boldsymbol{q}}^{s'} - \omega_{\boldsymbol{q}}^s\right)^2 + \left(\Gamma_{\boldsymbol{q}}^s + \Gamma_{\boldsymbol{q}}^{s'}\right)^2} \left(\Gamma_{\boldsymbol{q}}^s + \Gamma_{\boldsymbol{q}}^{s'}\right), \tag{4}$$

where the phonon lifetime in Eq. (1) is substituted as $\Gamma_{\boldsymbol{q}}^s = 1/\tau_\lambda$, including three-phonon (3ph) and four-phonon (4ph) scattering. The group velocity is replaced with a generalized form containing off-diagonal elements [8,32],

$$\boldsymbol{v}_{\boldsymbol{q}}^{s',s} = \frac{\left\langle \boldsymbol{e}_{\boldsymbol{q}}^s \middle| \frac{\partial D(\boldsymbol{q})}{\partial \boldsymbol{q}} \middle| \boldsymbol{e}_{\boldsymbol{q}}^{s'} \right\rangle}{\omega_{\boldsymbol{q}}^s + \omega_{\boldsymbol{q}}^{s'}}, \tag{5}$$

in which $\boldsymbol{e}_{\boldsymbol{q}}^s$ and $D(\boldsymbol{q})$ are the polarization vector and the phonon dynamical matrix, respectively. When $s = s'$, it stands for the phonon band diagonal terms, while $s \neq s'$ corresponds to the off-diagonal terms.

Therefore, the total lattice thermal conductivity $\kappa_L = \kappa_p + \kappa_c$. Note that, in order to compute the generalized group velocity correctly, we used the phase convention that accounts for atomic positions within its lattice point to construct the dynamical matrix, as adopted in earlier studies [37]. The details of the calculation are shown within the Supplemental Material [38–44].

III. RESULTS AND DISCUSSION

$CsPbBr_3$ is a typical phase change material of ABX_3 perovskite. One can discriminate the transition temperature by the dynamical instability of the appearance of soft acoustic phonons from anharmonic potential energy surfaces [45,46]. Specifically for $CsPbBr_3$, a second-order phase transition occurs at about 318 K and the transition temperature may vary, up to 361 K, depending on different samples. At about 373 K, there is another first-order phase transition. The critical temperature was also found at a higher temperature of about 401 K due to different experimental conditions [47,48]. Here, we have chosen an intermediate temperature by considering the above different experimental values [47,48]. Accordingly, the estimated temperatures for the first-order and second-order phase transitions are 320 K and 400 K, respectively. The high-temperature phase remains a cubic symmetry. The temperature reduction induces symmetry breaking, leading to anisotropic structures from the cubic to the tetragonal at midtemperature and finally to the orthorhombic crystals at low temperature [12,47–49]. All three crystal structures are depicted in Figs. 1(a)–1(c).

Figure 1(e) shows the effects of SCPH, 4ph, and κ_c on the calculated lattice thermal conductivity of $CsPbBr_3$. In the

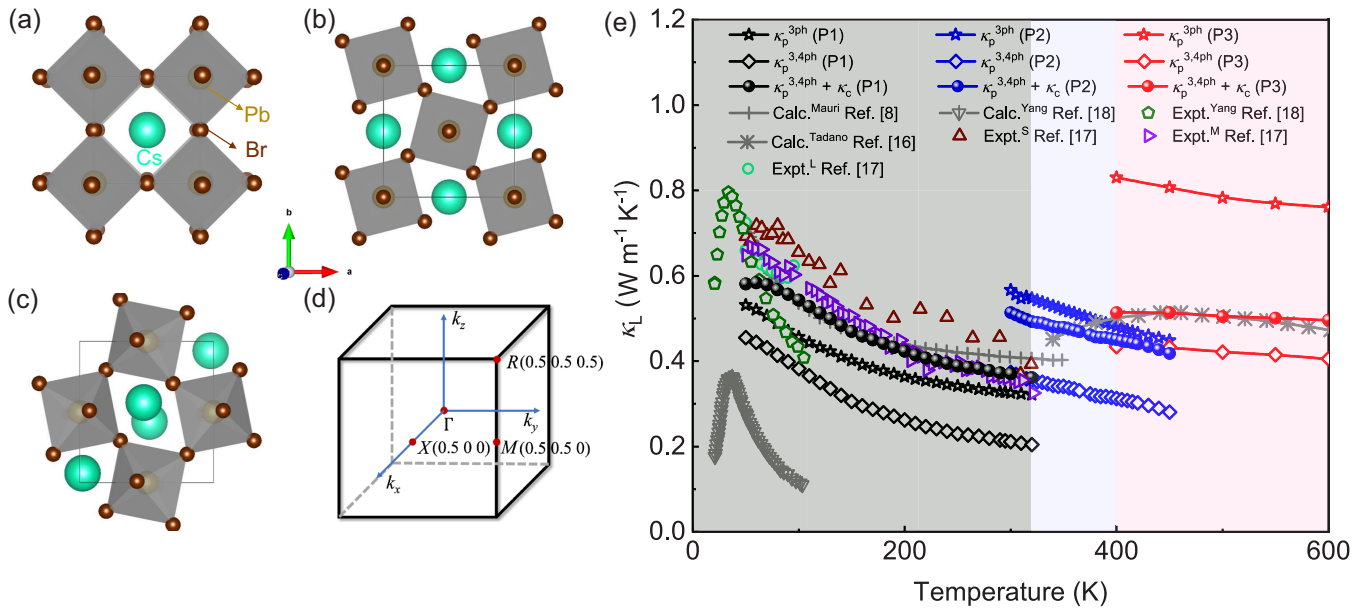

FIG. 1. (a)–(c) Crystal structures of $CsPbBr_3$ in the orthorhombic, tetragonal, and cubic phases, respectively. The green, brown, and yellow colors represent cesium (Cs), bromine (Br), and lead (Pb) atoms. (d) The first Brillouin zone of the cubic phase with high symmetry points Γ, X, M, and R indicated by red dots. (e) Lattice thermal conductivity κ_L of $CsPbBr_3$ includes diagonal and off-diagonal contributions in three phases using self-consistent phonon approximation. P1, P2, and P3 represent orthorhombic, tetragonal, and cubic phases. κ_p [Eq. (1)] is the standard Peierls contribution and κ_c [Eq. (4)] is the coherent contribution from the off-diagonal Wigner distribution elements. 3ph indicates only three-phonon scattering is included and 3,4ph means both three-phonon and four-phonon scattering are considered. For comparison, the unified first-principles theory [8] and the quasiparticle nonlinear theory (QP-NL) [9] are plotted for reference. Expt.^{L}, Expt.^{M}, and Expt.^{S} refer to experiments on single crystalline nanowires [21] with cross sections of 800 × 380 nm^2, 320 × 390 nm^2, and 300 × 160 nm^2, respectively.

following, we neglect the SCPH notation for simplicity. Different primitive cells are used to calculate the corresponding temperature range. Due to the different crystal symmetry, we find that κ_L increases from the orthorhombic to the tetragonal and the cubic phases. Moreover, $\kappa_p^{3,4ph} + \kappa_c$ in each phase decreases as temperature increases because of the enhanced phonon scattering. Since P1 and P2 are anisotropic, we use the arithmetic mean value in the figure.

Compared with κ_p^{3ph}, $\kappa_p^{3,4ph}$ is smaller due to the additional 4ph scattering. Moreover, the gap between them ($\Delta = \kappa_p^{3ph} - \kappa_p^{3,4ph}$) is growing significantly from P1 to P2 and finally to P3 based on Eq. (1). For instance, Δ is 0.114, 0.168, and 0.361 W m^{-1} K^{-1} for temperatures 300 K, 400 K, and 500 K, respectively. It is usually attributed to the different scaling laws of 4ph ($\tau_4^{-1} \sim T^2\omega^4$) and 3ph ($\tau_3^{-1} \sim T\omega^2$) scatterings in which τ is the relaxation time [50]. Therefore, 4ph scattering is more critical than 3ph scattering at high temperature and Δ is proportional to the temperature.

Since the ABX_3 perovskite has ultralow κ_L and off-diagonal terms contribute significantly [8,11], we include κ_c calculation of $CsPbBr_3$ based on Eq. (4) and Eq. (5). At 300 K, the value of κ_c of $CsPbBr_3$ for P1 phase is 0.158 W m^{-1} K^{-1}. At 400 K and 500 K, κ_c of $CsPbBr_3$ for both P2 and P3 phases are 0.138 and 0.084 W m^{-1} K^{-1}, respectively. More details of the values can be found in Supplemental Material S3 [38].

Our results of κ_c agree reasonably well with the one reported by Simoncelli, Marzari, and Mauri [8], while the minor deviations might come from the size of the supercell used in the calculation of harmonic phonon as well as additional effects arising from quartic anharmonicity. For the P3 phase, the value of ($\kappa_p^{3,4ph} + \kappa_c$) is 0.501 W m^{-1} K^{-1} at 500 K, which is quite close to the result of 0.50 W m^{-1} K^{-1} from the recent quasiparticle nonlinear theory (QP-NL) [9].

Next, we investigate the influence of anharmonic renormalization on phonon dispersion among orthorhombic, tetragonal, and cubic phases of $CsPbBr_3$. Phonon-phonon interaction and lattice anharmonicity are ascribable to the cubic, quartic, and even higher-order IFCs.

The phonon spectra at different temperatures in three phases are shown in Fig. 2. Unexpectedly, we notice that the acoustic and optical phonon branches become hardened as temperature increases for the low-temperature orthorhombic phase of $CsPbBr_3$, shown in Fig. 2(a). Nevertheless, it is indisputable for the high-temperature cubic phase that the acoustic branches stiffen, whereas the top three optical branches soften with increasing temperature, shown in Fig. 2(c). For the tetragonal phase of $CsPbBr_3$ in Fig. 2(b), the high-lying optical phonons are almost temperature independent. We also plot the off-diagonal term contribution for $CsPbBr_3$ heat transport of three phases, which can be found in the Supplemental Material [38].

We also analyze the frequency-resolved (dashed lines) and cumulative (solid lines) lattice thermal conductivity κ_L at different temperatures for cubic $CsPbBr_3$, shown in Figs. 2(d)–2(f). Since 4ph has proved to be additional

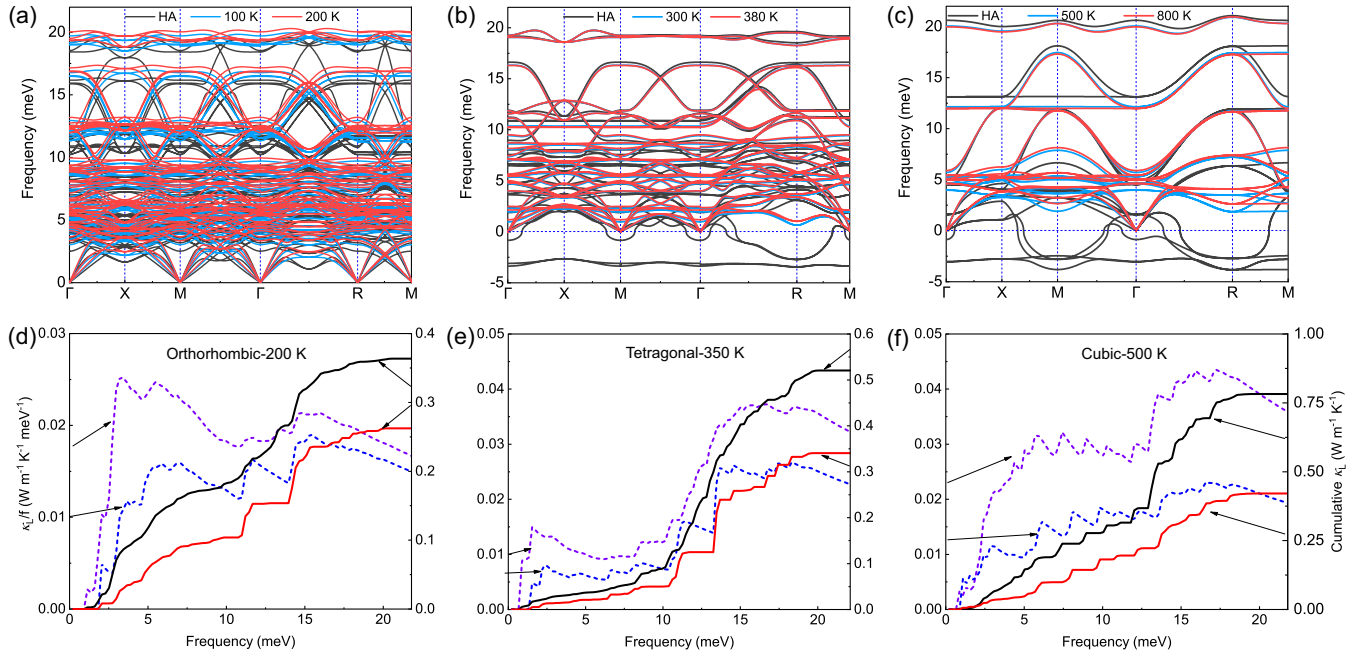

FIG. 2. Renormalized phonon dispersions for (a) orthorhombic, (b) tetragonal, and (c) cubic phases at different temperatures, respectively. HA is the harmonic approximation. Panels (d), (e), and (f) are the frequency-resolved κ_L (dashed lines) and cumulative κ_L (solid lines) using 3ph (the upper line) and 3,4ph (the lower line) methods at different temperatures, respectively.

scattering, κ_L of 3ph (the upper one) is more significant than that of 4ph (the lower one).

Traditionally, acoustic phonons are the main heat carriers. However, in cubic $CsPbBr_3$, it is found that optical phonons, ranging from 13.0 to 16.0 meV, dominate the heat transport, no matter whether or not the 4ph scattering processes are accounted for. Furthermore, 4ph scattering reduces κ_L of the cubic $CsPbBr_3$ by almost 40% on top of 3ph.

It is noticed that phonons of various frequencies dominate κ_L among different phases. Optical phonons above the frequency of 15.0 meV control the heat transport of 3ph and 4ph for the orthorhombic phase. In comparison, acoustic and optical phonons among the frequency of 3.0 meV and 6.0 meV are also important for 3ph transport. However, for the tetragonal phase, we can find that optical phonons among the frequency from 13.0 meV to 19.0 meV dominate the phonon transport of 3ph and 4ph as well.

Different phonon-temperature tendencies is an interesting phenomenon that has yet to be thoroughly investigated. Previous work only found consistently softened or hardened phonons [5,51] in different materials. We unveiled the multitendency of high-frequency phonon modes variation occurring in different phases of the same material. We reveal in the following that such an opposite tendency of optical phonon modes of cubic $CsPbBr_3$ as a function of temperature is sourced from the interaction between the top three opticals and other phonon modes.

In order to understand the underlying physical mechanism of the optical branches with high frequencies of different $CsPbBr_3$ phases having opposite temperature dependence in their phonon spectra, we have systematically studied the strength of 4ph interaction matrix elements $I_{\lambda\lambda_1}$ that have been introduced in Eq. (2) and Eq. (3). We set λ for the highest optical phonon mode as any mode of the three highest optical phonon branches (index of mode = 13–15 for cubic and 58–60 for the orthorhombic phase) and change λ_1 from the lowest acoustic phonon (index of mode = 1) to all other optical phonons, gradually scrutinizing the interaction between phonon population n_λ, quartic-anharmonicity $V^{(4)}(\lambda, -\lambda, \lambda_1, -\lambda_1)$, phonon frequencies Ω_{λ_1}, and Ω_λ, respectively. Here we use the imode parameter to label the index of the phonon branches.

Interestingly, $I_{\lambda\lambda_1}$ is mainly positive for the orthorhombic phase, as is shown in Fig. 3. It can be both positive and negative for the tetragonal phase and they almost cancel with each other leading to a small net frequency change. In contrast, it is found that the highest three optical branches have strong coupling with phonons in the low-frequency region and the interaction $I_{\lambda\lambda_1}$ is even negative in the cubic $CsPbBr_3$, shown in Fig. 3. We further examine the wave vector position behind the negative $I_{\lambda\lambda_1}$ and discover that most negative $I_{\lambda\lambda_1}$ stem from the low-energy acoustic phonon modes, especially around *M* and *R* high-symmetry points.

In Supplemental Material S9–S11 [38], we also show the $I_{\lambda\lambda_1}$ between imode = 3, 57 at 100 K for the P1 phase, imode = 3, 27 at 350 K for the P2 phase, and imode = 3, 12 at 500 K for the P3 phase, respectively. Since $I_{\lambda\lambda_1}$ can be either positive or negative, the renormalized phonon frequency Ω_λ as a function of temperature can either increase or decrease according to Eq. (2). Based on Eq. (3), only when $V^{(4)}(\lambda, -\lambda, \lambda_1, -\lambda_1)$ is negative for the three highest optical phonons of the cubic phase, leading to a negative $I_{\lambda\lambda_1}$ and a reduced renormalization phonon frequency based on Eq. (2). On the contrary, $I_{\lambda\lambda_1}$ is positive as a function of temperature for the orthorhombic phase and finally results in an increased Ω_λ. Owing to the strong interaction between low-energy phonon

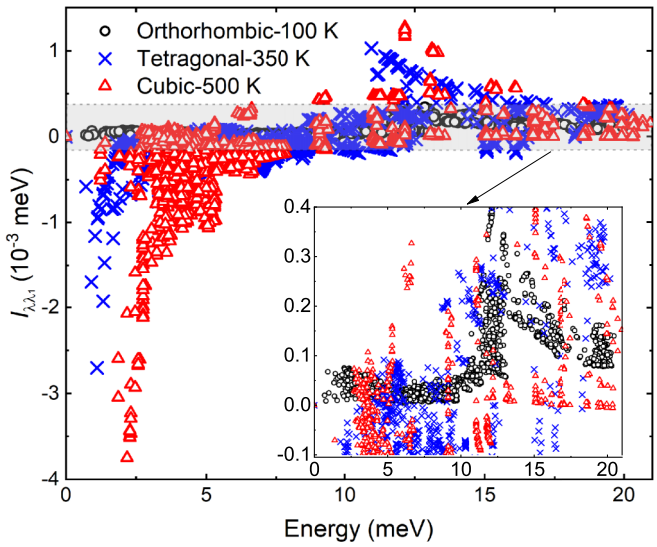

FIG. 3. Scattering strength $I_{\lambda\lambda_1}$ of the 4ph interaction matrix elements between the highest zone-center optical phonon mode and all other remaining phonons in three various phases according to Eq. (2) and Eq. (3) for the (a) orthorhombic at 100 K, (b) tetragonal at 350 K, and (c) cubic phase at 500 K, respectively.

modes around M and R and high-frequency optical phonons, the three highest optical phonon frequencies, with the temperature increasing, are softening for the cubic phase while hardening for the orthorhombic phase. More details can be found in the Supplemental Material [38].

To further understand the effects of anharmonic phonon renormalization and 4ph scattering on the thermal transport properties of $CsPbBr_3$, we continue to examine several parameters related to the lattice thermal conductivity, i.e., phonon phase space and scattering rates, respectively.

All available 3ph and 4ph scattering phase spaces need to satisfy the energy and quasimomentum conservation simultaneously [20,52], shown in Fig. 4(a). The phase space of 3ph and 4ph scatterings increases as the temperature rises from 500 K to 800 K. Since the unit of phase space of 3ph and 4ph is different, one cannot compare them directly. Nevertheless, the larger phase space means more available scattering channels. The scattering strength in each accessible channel determines the final phonon relaxation time. Therefore, by including 4ph scattering, the lattice thermal conductivity is generally smaller than that with only 3ph scattering.

The phonon scattering rates of the cubic phase are shown in Fig. 4(b). It displays that 4ph scattering has the same order of phonon scattering strength as that of 3ph. The scattering rates

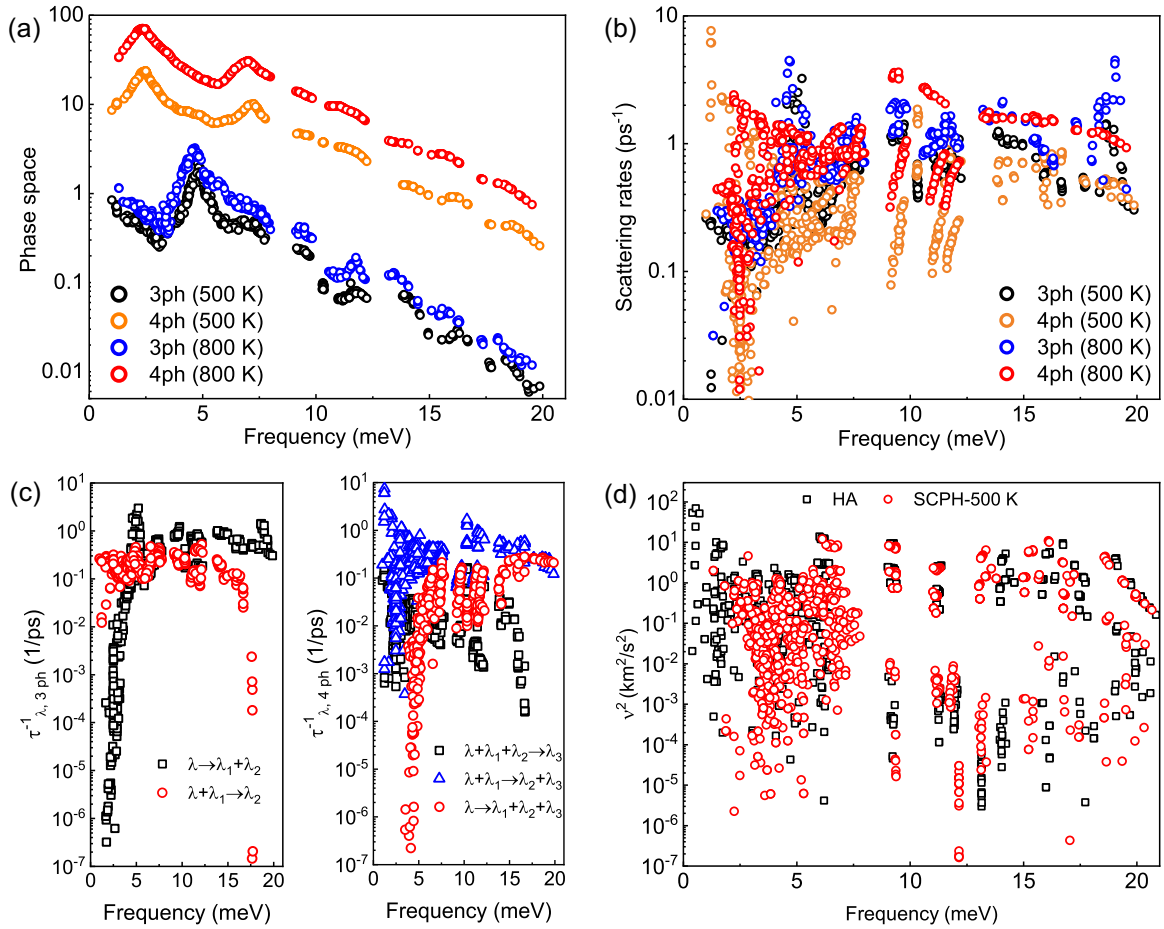

FIG. 4. (a) Phonon scattering phase space and (b) scattering rates between 3ph and 4ph for cubic $CsPbBr_3$ at different temperatures. (c) 3ph and 4ph scattering with channels resolution, including the splitting ($\lambda\rightarrow\lambda_1+\lambda_2$, $\lambda\rightarrow\lambda_1+\lambda_2+\lambda_3$), combination ($\lambda+\lambda_1\rightarrow\lambda_2$, $\lambda+\lambda_1+\lambda_2\rightarrow\lambda_3$), and redistribution ($\lambda+\lambda_1\rightarrow\lambda_2+\lambda_3$) processes at 500 K. (d) v^2, where v is phonon group velocity.

and phase space results for the orthorhombic and the tetragonal structures also show the same trends in Supplemental Material S5–S8 [38].

Figure 4(c) displays the absorption and emission processes of the 3ph and 4ph as a function of frequency at 500 K, respectively. For the 3ph scattering, we consider the phonon splitting ($\lambda \rightarrow \lambda_1 + \lambda_2$) and combination ($\lambda + \lambda_1 \rightarrow \lambda_2$). For the 4ph situation, we count both phonon splitting ($\lambda \rightarrow \lambda_1 + \lambda_2 + \lambda_3$) and combination ($\lambda + \lambda_1 + \lambda_2 \rightarrow \lambda_3$), as well as redistribution ($\lambda + \lambda_1 \rightarrow \lambda_2 + \lambda_3$) processes. In the low-frequency region wherein acoustic modes dominate, 3ph combination processes are stronger than the splitting situation, while the redistribution processes of 4ph are the dominant ones. However, in the high-frequency region that is dominated by optical modes, the splitting process of 3ph becomes more important. For 4ph scattering, the splitting process also increases to a dominating portion and has the same order as the redistribution process.

Figure 4(d) shows the temperature effect on v^2, where v is the group velocity at different temperatures for the cubic phase. Interestingly, v^2 of 800 K is higher than that of 500 K for most frequencies but almost the same for the acoustic phonons. It stems from the renormalized phonon dispersions at finite temperatures. Besides, we distinguish phonon group velocity for the cases with and without considering SCPH in Supplemental Material S4 [38].

Besides, for the ABX_3 perovskites, we find that dynamical stability is in line with the thermodynamic stability [53,54]. Previous work also used finite-temperature phonon dispersion of different phases of perovskites to predict the phase transition temperature [9]. But for other materials, dynamical stability and thermodynamical stability have no direct connection.

In general, the larger the lattice constant, the weaker the interatomic interaction in materials, which will usually lead to a lower lattice thermal conductivity. On the one hand, the calculation of three-phonon scattering including thermal expansion in lower temperature phases (orthorhombic phase and tetragonal phase) is computationally prohibitive since they have lower symmetry and more atoms in the primitive cell compared with the cubic phase. On the other hand, based on the experimental investigations, the coefficient of thermal expansion for $CsPbBr_3$ is 3.8×10^{-5} K^{-1}, 6.5×10^{-5} K^{-1}, and 2.6×10^{-5} K^{-1} for orthorhombic, tetragonal, and cubic phase, respectively [55]. The effect of the lattice constant on the thermal conductivity might be neglected in a moderate temperature range. Therefore, in our calculation, we neglect the thermal expansion like previous works [8,11,12]. Most recently, an effective one-body Hamiltonian that well represents the quasiparticle peak has been developed. In this method, the thermal expansion in the calculation is included [9].

IV. CONCLUSIONS

In summary, our study reveals the significant contributions of four-phonon scattering and the off-diagonal terms of the heat flux operators in calculating the thermal conductivity in systems with harmonic phonons exhibiting imaginary frequencies and temperature renormalization.

Specifically, our investigation of $CsPbBr_3$ halide perovskites in orthorhombic, tetragonal, and cubic phases yields the following key findings.

(i) For materials with ultralow lattice thermal conductivity κ_L, the inclusion of high-order anharmonicity and off-diagonal terms bridges the gap between experimental observations and theoretical predictions.

(ii) The strong coupling between high-frequency optical phonons and overdamped acoustic phonons ($I_{\lambda\lambda_1}$) provides insights into the intriguing phonon renormalization phenomena observed in strongly anharmonic systems as a function of temperature.

(iii) Beyond the conventional phonon-phonon scattering perspective, phenomena such as electron-phonon coupling, polaron formation, and entropy in halide perovskites warrant further theoretical advancements [12,56].

Our study, which presents an effective approach to understanding the ultralow κ_L observed in halide perovskites, might inspire further experimental investigations exploring materials with glasslike thermal conductivity.

ACKNOWLEDGMENTS

We acknowledge the support from the National Natural Science Foundation of China (Grants No. 12104356 and No. 52250191). Z.G. acknowledges the support of the China Postdoctoral Science Foundation (Grant No. 2022M712552) and the Fundamental Research Funds for the Central Universities. We also acknowledge the support by State Key Laboratory for Mechanical Behavior of Materials and HPC Platform, Xi'an Jiaotong University. Y.X. acknowledges the Portland State University Lab Setup Fund.

[1] A. Togo, L. Chaput, and I. Tanaka, Distributions of phonon lifetimes in Brillouin zones, Phys. Rev. B **91**, 094306 (2015).

[2] J. Carrete, W. Li, N. Mingo, S. Wang, and S. Curtarolo, Finding Unprecedentedly Low-Thermal-Conductivity Half-Heusler Semiconductors via High-Throughput Materials Modeling, Phys. Rev. X **4**, 011019 (2014).

[3] A. van Roekeghem, J. Carrete, C. Oses, S. Curtarolo, and N. Mingo, High-Throughput Computation of Thermal Conductivity of High-Temperature Solid Phases: The Case of Oxide and Fluoride Perovskites, Phys. Rev. X **6**, 041061 (2016).

[4] T. Tadano and S. Tsuneyuki, Self-consistent phonon calculations of lattice dynamical properties in cubic $SrTiO_3$ with first-principles anharmonic force constants, Phys. Rev. B **92**, 054301 (2015).

[5] Y. Zhao, S. Zeng, G. Li, C. Lian, Z. Dai, S. Meng, and J. Ni, Lattice thermal conductivity including phonon frequency shifts and scattering rates induced by quartic anharmonicity in cubic oxide and fluoride perovskites, Phys. Rev. B **104**, 224304 (2021).

[6] Y. Xia, V. I. Hegde, K. Pal, X. Hua, D. Gaines, S. Patel, J. He, M. Aykol, and C. Wolverton, High-Throughput Study of Lat-

tice Thermal Conductivity in Binary Rocksalt and Zinc Blende Compounds Including Higher-Order Anharmonicity, Phys. Rev. X **10**, 041029 (2020).

[7] J. S. Kang, H. Wu, M. Li, and Y. Hu, Intrinsic low thermal conductivity and phonon renormalization due to strong anharmonicity of single-crystal tin selenide, Nano Lett. **19**, 4941 (2019).

[8] M. Simoncelli, N. Marzari, and F. Mauri, Unified theory of thermal transport in crystals and glasses, Nat. Phys. **15**, 809 (2019).

[9] T. Tadano and W. A. Saidi, First-Principles Phonon Quasiparticle Theory Applied to a Strongly Anharmonic Halide Perovskite, Phys. Rev. Lett. **129**, 185901 (2022).

[10] S. Hu, Z. Ren, A. B. Djurisic, and A. L. Rogach, Metal halide perovskites as emerging thermoelectric materials, ACS Energy Lett. **6**, 3882 (2021).

[11] W. Lee, H. Li, A. B. Wong, D. Zhang, M. Lai, Y. Yu, Q. Kong, E. Lin, J. J. Urban, J. C. Grossman, and P. Yang, Ultralow thermal conductivity in all-inorganic halide perovskites, Proc. Natl. Acad. Sci. U.S.A. **114**, 8693 (2017).

[12] T. Lanigan-Atkins, X. He, M. J. Krogstad, D. M. Pajerowski, D. L. Abernathy, G. N. M. N. Xu, Z. Xu, D.-Y. Chung, M. G. Kanatzidis, S. Rosenkranz, R. Osborn, and O. Delaire, Two-dimensional overdamped fluctuations of the soft perovskite lattice in $CsPbBr_3$, Nat. Mater. **20**, 977 (2021).

[13] S. Svirskas, S. Balciunas, M. Simenas, G. Usevicius, M. Kinka, M. Velicka, D. Kubicki, M. E. Castillo, A. Karabanov, V. V. Shvartsman, M. de Rosario Soares, V. Sablinskas, A. N. Salak, D. C. Lupascu, and J. Banys, Phase transitions, screening and dielectric response of $CsPbBr_3$, J. Mater. Chem. A **8**, 14015 (2020).

[14] F. Zhou, W. Nielson, Y. Xia, and V. Ozoliņš, Lattice Anharmonicity and Thermal Conductivity from Compressive Sensing of First-Principles Calculations, Phys. Rev. Lett. **113**, 185501 (2014).

[15] F. Zhou, W. Nielson, Y. Xia, and V. Ozoliņš, Compressive sensing lattice dynamics. I. General formalism, Phys. Rev. B **100**, 184308 (2019).

[16] F. Zhou, B. Sadigh, D. Åberg, Y. Xia, and V. Ozoliņš, Compressive sensing lattice dynamics. II. Efficient phonon calculations and long-range interactions, Phys. Rev. B **100**, 184309 (2019).

[17] T. Feng and X. Ruan, Quantum mechanical prediction of four-phonon scattering rates and reduced thermal conductivity of solids, Phys. Rev. B **93**, 045202 (2016).

[18] L. Isaeva, G. Barbalinardo, D. Donadio, and S. Baroni, Modeling heat transport in crystals and glasses from a unified lattice-dynamical approach, Nat. Commun. **10**, 3853 (2019).

[19] A. Debernardi, S. Baroni, and E. Molinari, Anharmonic Phonon Lifetimes in Semiconductors from Density-Functional Perturbation Theory, Phys. Rev. Lett. **75**, 1819 (1995).

[20] Z. Gao, F. Tao, and J. Ren, Unusually low thermal conductivity of atomically thin 2D tellurium, Nanoscale **10**, 12997 (2018).

[21] Y. Wang, R. Lin, P. Zhu, Q. Zheng, Q. Wang, D. Li, and J. Zhu, Cation dynamics governed thermal properties of lead halide perovskite nanowires, Nano Lett. **18**, 2772 (2018).

[22] N. Li, B. Li, and S. Flach, Energy Carriers in the Fermi-Pasta-Ulam β Lattice: Solitons or Phonons?, Phys. Rev. Lett. **105**, 054102 (2010).

[23] P. Souvatzis, O. Eriksson, M. I. Katsnelson, and S. P. Rudin, Entropy Driven Stabilization of Energetically Unstable Crystal Structures Explained from First Principles Theory, Phys. Rev. Lett. **100**, 095901 (2008).

[24] I. Errea, B. Rousseau, and A. Bergara, Anharmonic Stabilization of the High-Pressure Simple Cubic Phase of Calcium, Phys. Rev. Lett. **106**, 165501 (2011).

[25] I. Errea, M. Calandra, and F. Mauri, Anharmonic free energies and phonon dispersions from the stochastic self-consistent harmonic approximation: Application to platinum and palladium hydrides, Phys. Rev. B **89**, 064302 (2014).

[26] Y. Xia, Revisiting lattice thermal transport in PbTe: The crucial role of quartic anharmonicity, Appl. Phys. Lett. **113**, 073901 (2018).

[27] N. K. Ravichandran and D. Broido, Phonon-Phonon Interactions in Strongly Bonded Solids: Selection Rules and Higher-Order Processes, Phys. Rev. X **10**, 021063 (2020).

[28] B. S. Semwal and P. K. Sharma, Thermal conductivity of an anharmonic crystal, Phys. Rev. B **5**, 3909 (1972).

[29] D. C. Knauss and R. S. Wilson, Theory of thermal conductivity of anharmonic crystals: Nondiagonal Peierls contribution, Phys. Rev. B **10**, 4383 (1974).

[30] G. P. Srivastava and M. Prasad, Diagonal and nondiagonal Peierls contribution to the thermal conductivity of anharmonic crystals, Phys. Rev. B **23**, 4273 (1981).

[31] P. B. Allen and J. L. Feldman, Thermal Conductivity of Glasses: Theory and Application to Amorphous Si, Phys. Rev. Lett. **62**, 645 (1989).

[32] P. B. Allen and J. L. Feldman, Thermal conductivity of disordered harmonic solids, Phys. Rev. B **48**, 12581 (1993).

[33] A. Cepellotti and N. Marzari, Thermal Transport in Crystals as a Kinetic Theory of Relaxons, Phys. Rev. X **6**, 041013 (2016).

[34] X. Chen, A. Weathers, J. Carrete, S. Mukhopadhyay, O. Delaire, D. A. Stewart, N. Mingo, S. N. Girard, J. Ma, D. L. Abernathy, J. Yan, R. Sheshka, D. P. Sellan, F. Meng, S. Jin, J. Zhou, and L. Shi, Twisting phonons in complex crystals with quasi-one-dimensional substructures, Nat. Commun. **6**, 6723 (2015).

[35] P.-F. Lory, S. Pailhes, V. M. Giordano, H. Euchner, H. D. Nguyen, R. Ramlau, H. Borrmann, M. Schmidt, M. Baitinger, M. Ikeda, P. Tomeš, M. Mihalkovič, C. Allio, M. R. Johnson, H. Schober, Y. Sidis, F. Bourdarot, L. P. Regnault, J. Ollivier, S. Paschen, Y. Grin, and M. de Boissieu, Direct measurement of individual phonon lifetimes in the clathrate compound $Ba_{7.81}Ge_{40.67}Au_{5.33}$, Nat. Commun. **8**, 491 (2017).

[36] S. Mukhopadhyay, D. S. Parker, B. C. Sales, A. A. Puretzky, M. A. McGuire, and L. Lindsay, Two-channel model for ultralow thermal conductivity of crystalline Tl_3VSe_4, Science **360**, 1455 (2018).

[37] A. Auerbach and P. B. Allen, Universal high-temperature saturation in phonon and electron transport, Phys. Rev. B **29**, 2884 (1984).

[38] See Supplemental Material at http://link.aps.org/supplemental/10.1103/PhysRevB.107.214308 for the details of calculated lattice constants using different exchange-correlation functionals compared with the experimental data, convergence test with sampling grid, matrix parameters for the phonon-phonon interaction, and off-diagonal term contribution for three phases of $CsPbBr_3$.

[39] G. Kresse and J. Furthmüller, Efficient iterative schemes for *ab initio* total-energy calculations using a plane-wave basis set, Phys. Rev. B **54**, 11169 (1996).

[40] P. E. Blöchl, Projector augmented-wave method, Phys. Rev. B **50**, 17953 (1994).

[41] G. Kresse and D. Joubert, From ultrasoft pseudopotentials to the projector augmented-wave method, Phys. Rev. B **59**, 1758 (1999).

[42] K. Esfarjani and H. T. Stokes, Method to extract anharmonic force constants from first principles calculations, Phys. Rev. B **77**, 144112 (2008).

[43] A. Togo and I. Tanaka, First principles phonon calculations in materials science, Scr. Mater. **108**, 1 (2015).

[44] E. J. Candes and M. B. Wakin, An introduction to compressive sampling, IEEE Signal Process. Mag. **25**, 21 (2008).

[45] X. He, D. Bansal, B. Winn, S. Chi, L. Boatner, and O. Delaire, Anharmonic Eigenvectors and Acoustic Phonon Disappearance in Quantum Paraelectric $SrTiO_3$, Phys. Rev. Lett. **124**, 145901 (2020).

[46] V. Krapivin, M. Gu, D. Hickox-Young, S. W. Teitelbaum, Y. Huang, G. de la Peña, D. Zhu, N. Sirica, M.-C. Lee, R. P. Prasankumar, A. A. Maznev, K. A. Nelson, M. Chollet, J. M. Rondinelli, D. A. Reis, and M. Trigo, Ultrafast Suppression of the Ferroelectric Instability in $KTaO_3$, Phys. Rev. Lett. **129**, 127601 (2022).

[47] M. Natarajan and B. Prakash, Phase transitions in ABX_3 type halides, Phys. Status Solidi A **4**, K167 (1971).

[48] D. Malyshkin, V. Sereda, I. Ivanov, M. Mazurin, A. Sednev-Lugovets, D. Tsvetkov, and A. Zuev, New phase transition in $CsPbBr_3$, Mater. Lett. **278**, 128458 (2020).

[49] J. S. Bechtel, J. C. Thomas, and A. Van der Ven, Finite-temperature simulation of anharmonicity and octahedral tilting transitions in halide perovskites, Phys. Rev. Mater. **3**, 113605 (2019).

[50] T. Feng, L. Lindsay, and X. Ruan, Four-phonon scattering significantly reduces intrinsic thermal conductivity of solids, Phys. Rev. B **96**, 161201(R) (2017).

[51] J. Zheng, D. Shi, Y. Yang, C. Lin, H. Huang, R. Guo, and B. Huang, Anharmonicity-induced phonon hardening and phonon transport enhancement in crystalline perovskite $BaZrO_3$, Phys. Rev. B **105**, 224303 (2022).

[52] L. Lindsay and D. A. Broido, Three-phonon phase space and lattice thermal conductivity in semiconductors, J. Phys.: Condens. Matter **20**, 165209 (2008).

[53] J. Yang and S. Li, An atlas of room-temperature stability and vibrational anharmonicity of cubic perovskites, Mater. Horiz. **9**, 1896 (2022).

[54] Q. Sun and W. J. Yin, Thermodynamic stability trend of cubic perovskites, J. Am. Chem. Soc. **139**, 14905 (2017).

[55] T. Haeger, R. Heiderhoff, and T. Riedl, Thermal properties of metal-halide perovskites, J. Mater. Chem. C **8**, 14289 (2020).

[56] J. J. Zhou, O. Hellman, and M. Bernardi, Electron-Phonon Scattering in the Presence of Soft Modes and Electron Mobility in $SrTiO_3$ Perovskite from First Principles, Phys. Rev. Lett. **121**, 226603 (2018).